

CT characteristics and pathological implications of early stage (T1N0M0) lung adenocarcinoma with pure ground-glass opacity

Xin Jin · Shao-hong Zhao · Jie Gao · Dian-jun Wang ·
Jian Wu · Chong-chong Wu · Rui-ping Chang ·
Hai-yue Ju

Received: 4 November 2014 / Accepted: 21 January 2015 / Published online: 1 March 2015
© European Society of Radiology 2015

Abstract

Objectives To analyze the CT characteristics and pathological classification of early lung adenocarcinoma (T1N0M0) with pure ground-glass opacity (pGGO).

Methods Ninety-four lesions with pGGO on CT in 88 patients with T1N0M0 lung adenocarcinoma were selected from January 2010 to December 2012. All lesions were confirmed by pathology. CT appearances were analyzed including lesion location, size, density, uniformity, shape, margin, tumour-lung interface, internal and surrounding malignant signs. Lesion size and density were compared using analysis of variance, lesion size also assessed using ROC curves. Gender of patients, lesion location and CT appearances were compared using χ^2 -test.

Results There were no significant differences in gender, lesion location and density with histological invasiveness ($P>0.05$). The ROC curve showed that the possibility of invasive lesion was 88.73 % when diameter of lesion was more than 10.5 mm. There was a significant difference between lesion uniformity and histological invasiveness ($P=0.01$). There were significant differences in margin, tumour-lung interface, air bronchogram with histological invasiveness ($P=0.02, P=0.00, P=0.048$). The correlation index of lesion size and uniformity was $r=0.45$ ($P=0.00$).

Conclusions The lesion size and uniformity, tumour-lung interface and the air bronchogram can help predict invasive extent of early stage lung adenocarcinoma with pGGO.

Key Points

- CT characteristics and pathological classification of pGGO lung adenocarcinoma smaller than 3 cm
- The optimal cut-off value for discriminating preinvasive from invasive lesions was 10.5 mm
- Uniformity was significant difference between histological subtypes and correlated with lesion size
- Tumour margin, tumour-lung interface and air bronchogram showed different between histological types
- No significant difference in gender, lesion location and density with histological subtypes

Keywords Lung neoplasms · Adenocarcinoma · Pathology · Tomography, X-ray computed · Ground glass opacity

Abbreviations

pGGO	pure ground-glass opacity
AAH	atypical adenomatous hyperplasia
AIS	adenocarcinoma in situ
MIA	invasive adenocarcinoma
BAC	bronchioloalveolar adenocarcinoma
ANOVA	one-way analysis of variance

Introduction

Adenocarcinoma is the most common histological type of lung cancer [1]. In 2011, a new classification of lung adenocarcinoma was proposed by an international multidisciplinary committee sponsored by the International Association for the Study of Lung Cancer (IASLC), the

X. Jin · S.-h. Zhao (✉) · J. Wu · C.-c. Wu · R.-p. Chang · H.-y. Ju
Department of Radiology, Chinese PLA General Hospital,
Beijing 100853, China
e-mail: cjr.zhaoshaohong@vip.163.com

J. Gao · D.-j. Wang
Department of Pathology, Chinese PLA General Hospital,
Beijing 100853, China

American Thoracic Society (ATS), and the European Respiratory Society (ERS) [2]. This classification addresses recent advances in oncology, molecular biology, pathology, radiology, and surgery of lung adenocarcinoma. For resection specimens, new concepts are introduced such as adenocarcinoma in situ (AIS) and minimally invasive adenocarcinoma (MIA) for small solitary adenocarcinomas with either pure lepidic growth (AIS) or predominant lepidic growth with ≤ 5 mm invasion (MIA) to define patients who, if they undergo complete resection, will have 100 % or near 100 % disease-specific survival, respectively. AIS and MIA are usually nonmucinous but rarely may be mucinous. Invasive adenocarcinomas are classified by a predominant pattern after using comprehensive histologic subtyping with lepidic (formerly most mixed subtype tumours with nonmucinous BAC), acinar, papillary, and solid patterns. Micropapillary has been added as a new histological subtype. Variants include invasive mucinous adenocarcinoma (formerly mucinous BAC), colloid, fetal, and enteric adenocarcinoma. This new classification especially affects computed tomographic (CT) diagnosis of lung adenocarcinoma. Lee and Godoy et al. [3, 4] reported that the most common CT findings of the new classification of lung adenocarcinoma as follows: AAH: pure ground-glass nodule (GGN); nonmucinous AIS: typically a pure GGN, sometimes a part-solid; nonmucinous MIA: a part-solid nodule with a predominant ground-glass component; LPA: a part-solid mass with variable proportion of ground-glass components or solid nodule; and another subtype predominant in adenocarcinoma: usually a solid mass or part-solid nodule (with predominant solid component). Those CT characteristics were determined mostly dependent on the studies before the new purposed classification. The radiologic-pathologic correlation under the 2011 classification was not fully established. The aim of this study was to clarify the correlation between CT findings of early stage lung adenocarcinoma (T1N0M0) with pure ground-glass opacity (GGO) and the new IASLC classification.

Materials and methods

Patients From January 2010 to December 2012, nearly 3,500 consecutive patients with lung adenocarcinoma in our hospital, who underwent a complete surgical resection, were reviewed. Only lesions presenting pGGO on CT and with clinical stage of T1N0M0 were selected. Ninety-four lesions in 88 patients (82 patients had a single lesion and six had two lesions) met the inclusion criteria. There were 33 male and 55 female patients (average age, 57.13 years; range, 26 to 78 years).

Image acquisition and analysis

CT was performed by using Somatom Sensation-64 (Siemens Medical Systems, Germany) with 120kVp and 100mAs. All images were reconstructed with a section thickness of 1.5 mm and displayed at a lung window width of 1600HU, window level of -600HU, and a mediastinal window width of 350HU, with a window level of 35HU. CT characteristics were analyzed by the consensus of two experienced thoracic radiologists (Zhao SH, Wu CC, with 20 and 16 years of experience in chest CT, respectively) who worked together on PACS with measurement done by Dr. Zhao or Wu. The location, size, CT attenuation, uniformity, shape, margin, internal and surrounding malignant signs of the nodules, and tumour-lung interface were recorded. The nodule size was the maximal diameter of the lesion on axial images. The average CT attenuation (HU) was measured by placing a region of interest (ROI) of 15 mm² in three different sites within the nodule barring the vessels and bronchioles. The uniformity was described as homogeneous, less homogeneous, and of heterogeneous density. No bubble-like lucency within the nodule was defined as homogeneous density, more than three lucency areas was defined as heterogeneous density and less homogeneous density was defined between the above two situations. The shape

Table 1 Lesion location of all nodules*

Pathologic group	Location					Sum
	Right upper lobe	Right middle lobe	Right lower lobe	Left upper lobe	Left lower lobe	
Preinvasive lesion	9	3	2	2	4	20
MIA (minimally invasive adenocarcinoma)	13	4	5	8	5	35
Invasive adenocarcinoma	11	4	7	9	7	38
Sum	33	11	14	19	16	93

*Except one growing across two lobes

($P=0.69, P>0.05$)

MIA: minimally invasive adenocarcinoma

Fig. 1 Distribution histogram of lesion size in three groups (A) Preinvasive lesions: main distribution range was 5.0–10.0 mm, peak point was 7.0 mm; (B) MIAs: main distribution range was 10.0–15.0 mm, peak point was 10.0 mm; (C) invasive adenocarcinomas: main distribution range was 20.0–22.5 mm, peak point was 20.0 mm

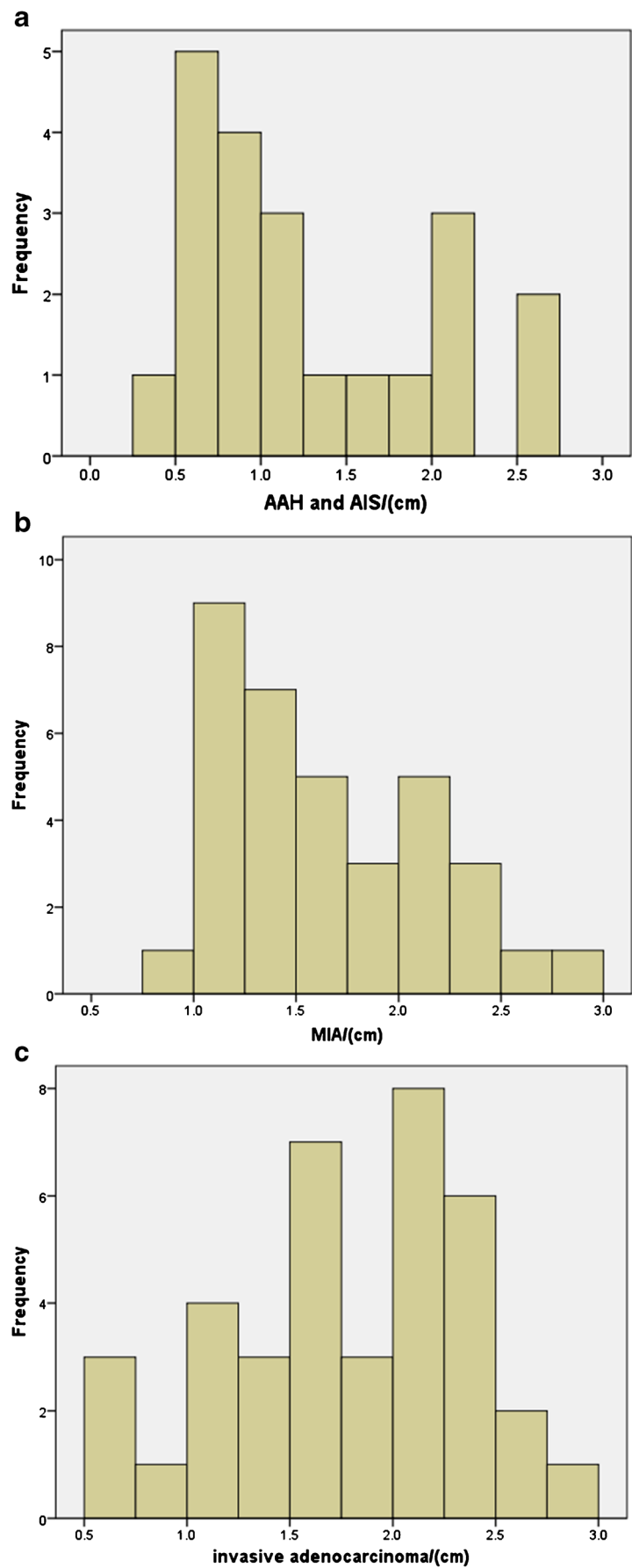
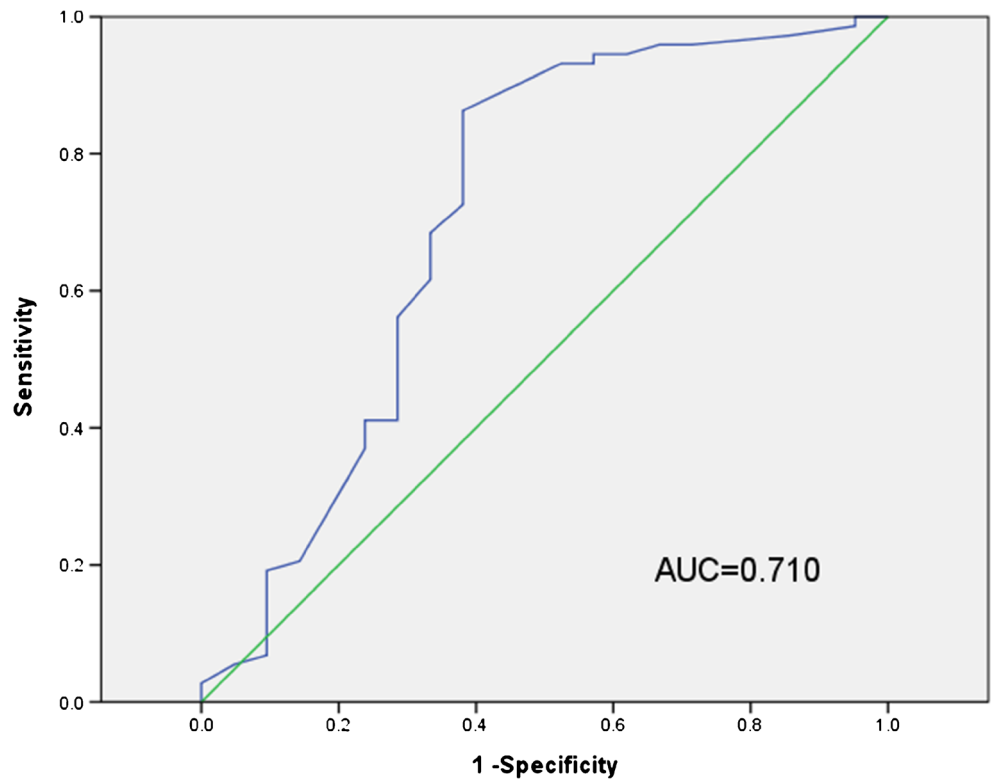


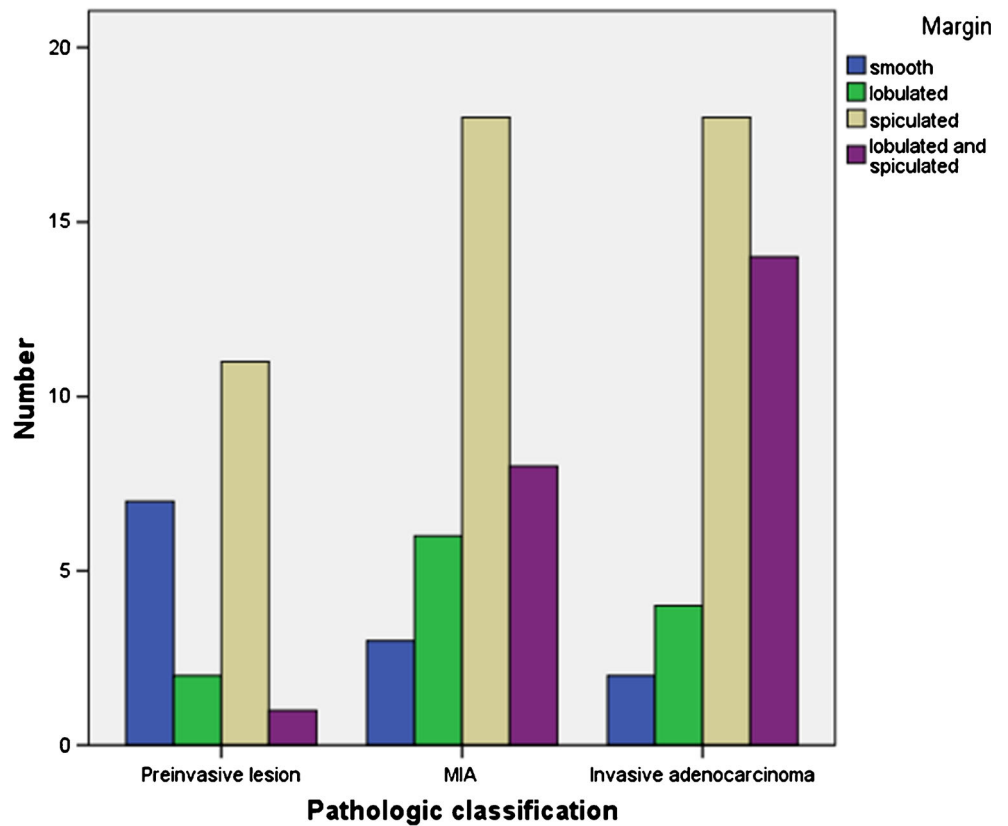
Fig. 2 A receiver operating characteristic curve of lesion size



of nodules was described as round, oval, polygonal, and irregular. The margin was described as smooth, lobulated,

spiculated, and lobulated with spiculation. Tumour-lung interface was recorded as well-demarcated or ill-

Fig. 3 Bar chart of lesion marginal characteristics in different pathological subtypes



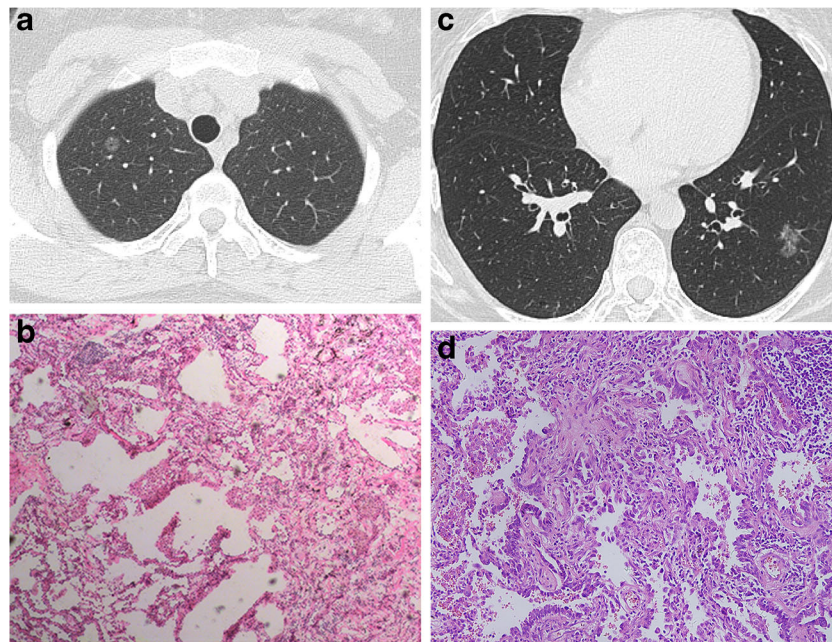


Fig. 4 Marginal characteristics of pGGO nodules (A) AIS in a 64-year-old woman, 1.5 mm thin-section CT image showed a smooth nodule located in the right upper lobe (B) Histopathologic photomicrograph (haematoxylin-eosin stain; magnification, $\times 100$) showed tumour cell growing restricted to alveolar walls (arrow) without stromal, vascular,

and pleural invasion. (C) LPA in a 50-year-old woman, 1.5 mm thin-section CT lung window showed a lobulated and spiculated nodule in the left lower lobe. (D) Histopathologic photomicrograph (haematoxylin-eosin stain; magnification, $\times 100$) showed tumour cell growing along alveolar and with a infiltrative growth pattern (arrow), invasion >5 mm

demarcated. The internal and surrounding malignant signs included bubble sign, air bronchogram, and pleural tags. Multiple GGO nodules in one patient were considered as

independent primary lesions. According to the IASLC/ATS/ERS classification, all lesions were categorized as

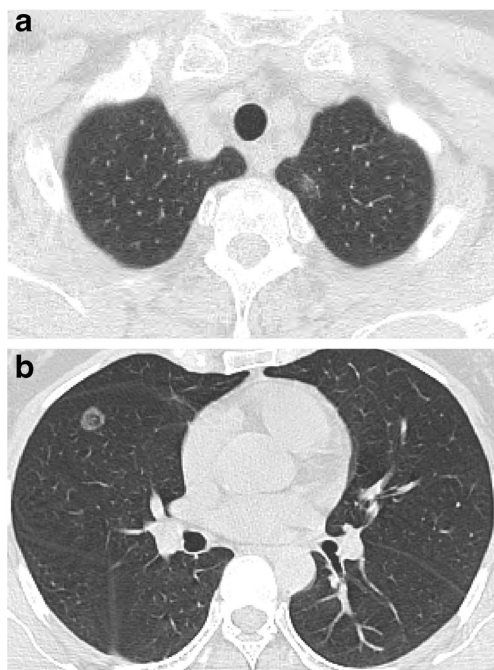


Fig. 5 Tumour-lung interface features of nodules (Transverse lung-window, thin-section 1.5 mm) (A) AAH lesion in a 59-year-old woman, an ill-defined nodule located in the left upper lobe. (B) LPA in a 41-year-old woman, a nodule with well-defined tumour-lung interface located in the right middle lobe

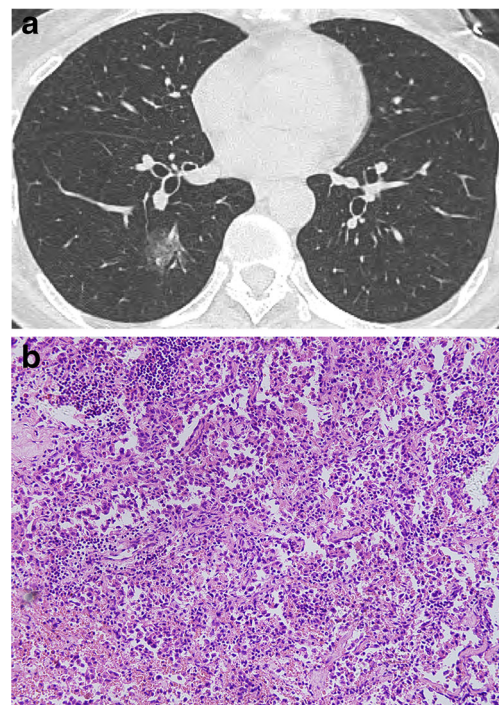


Fig. 6 (A) CT (Transverse lung-window, thin-section 1.5 mm) showed a pGGO nodule with air bronchogram in the right lower lobe in a 49-year-old man (B) Histopathologic photomicrograph proved to be LPA with a tumour cell growing infiltrate stroma, invasion >5 mm (haematoxylin-eosin stain; magnification, $\times 100$)

preinvasive lesions: atypical adenomatous hyperplasia (AAH) and adenocarcinoma in situ (AIS); minimally invasive adenocarcinoma (MIA); and invasive adenocarcinoma (including lepidic, acinar, papillary, solid and micropapillary predominant adenocarcinomas)

Statistical analysis Statistical analysis was performed with SPSS software (version 18.0). The correlation of nodule size and CT value with histological invasiveness were analyzed by using one-way analysis of variance (ANOVA). The Student-Newman-Keuls test and Kruskal-Wallis test were used depending on the homogeneity of variance. The correlation of patient’s sex, nodule location, CT findings (shape, margin, tumour-lung interface, internal and surrounding characteristics) with histological invasiveness were analyzed by using the Pearson χ^2 test and Fisher exact test. The optimal cut-off value of lesion size between preinvasive lesions and invasive lesions (MIA and invasive adenocarcinoma) was calculated by using a receiver operating characteristic (ROC) curve. Correlation analysis was used for the relationship between lesion size and lesion uniformity. A *P* value of less than 0.05 was considered to be a significant difference.

Results

Of the 94 nodules, there were 21 preinvasive lesions (seven AAHs and 14 AISs) (M:F=6:15), 35 MIAs (M:F=14:21), 38 invasive adenocarcinomas (M:F=14:24) including 27 lepidic predominant, four acinar predominant, three papillary predominant, one micropapillary predominant, and three solid predominant lesions. There were no significant differences in sex ratio and lesion location among preinvasive lesions, MIAs and invasive adenocarcinomas (*P*=0.69 and 0.37, *P*>0.05) (Table 1). The mean diameter of preinvasive lesions was 12.4±6.8 mm (peak point: 7.0 mm), that of MIAs was 16.0±5.2 mm (peak point: 10.0 mm), and that of invasive adenocarcinomas was 17.5±5.8 mm (peak point: 20.0 mm) (*P*=0.008, *P*<0.05) (Fig. 1). ROC analysis revealed that the AUC for lesion size was 0.710 (95 % CI: 0.561-0.860). The optimal cut-off value for lesion size in differentiating preinvasive lesions from invasive lesions was 10.5 mm, with a sensitivity of 86.30 %, a specificity of 61.90 %, a positive predictive value of 88.73 %, a negative predictive value of 56.52 %, and an accuracy of 80.85 %, respectively (Fig. 2). The mean CT value was (-531.0±84.6) HU for preinvasive lesions, (-492.7±127.2) HU

Table 2 CT Findings of all pGGO nodules

Characteristic	Preinvasive lesion <i>n</i> =(21)	MIA (minimally invasive adenocarcinoma) <i>n</i> =(35)	Invasive adenocarcinoma <i>n</i> =(38)	<i>P</i> value
Lesion size (mm)*	12.4±6.8	16.0±5.2	17.5±5.8	0.008 ⁺
CT attenuation (HU)*	-(531.0±84.6)	-(492.7±127.2)	-(512.4±109.4)	0.39 ⁺
Uniformity				0.01 [§]
Homogenous	8	15	3	
Less homogenous	11	16	18	
Heterogeneous	2	4	17	
Shape				0.17 [§]
Round	11	10	9	
Oval	5	11	7	
Polygonal	2	8	11	
Irregular	3	6	11	
Margin				0.02 [§]
Smooth	7	3	2	
Lobulated	2	6	4	
Spiculated	11	18	18	
Lobulated and spiculated	1	8	14	
Tumour-lung interface				0.00 [§]
Well-defined	8	27	33	
Ill-defined	13	8	5	
Internal and surrounding characteristics				
Bubble sign	11	24	25	0.13 [§]
Air bronchogram	2	7	14	0.048 [§]
Pleural tag	11	15	20	0.66 [§]

Note.—Except where indicated, data are the number of nodules
 *Data are means ± standard deviation
 § Fisher exact test
 + ANOVA: analysis of variance
 pGGO: pure ground-glass opacity

for MIAs, and (-512.4 ± 109.4) HU for invasive adenocarcinomas. There were no significant differences among preinvasive lesions, MIAs, and invasive adenocarcinomas ($P=0.39, P>0.05$). There was 38.10 % of homogeneity, 52.38 % of less homogeneity and 9.52 % of heterogeneity in preinvasive lesions; 42.86 % of homogeneity, 45.71 % of less homogeneity, and 11.43 % of heterogeneity in MIAs; 7.89 % of homogeneity, 47.37 % of less homogeneity and 44.74 % of heterogeneity in invasive adenocarcinomas. The uniformity of lesions in three groups showed significant differences ($P=0.01, P<0.05$). The lesion size was closely related with lesion uniformity, correlation index was $r=0.45$ ($P=0.00, P<0.05$).

The morphologic characteristics of nodules regarding the margin, tumour-lung interface, and air bronchogram sign were significantly different among preinvasive lesions, MIAs, and invasive adenocarcinomas ($P=0.02, P=0.00, P=0.048$,

respectively, $P<0.05$). The spiculation sign was demonstrated in 52.38 % of preinvasive lesions, 51.43 % of MIAs, and 47.37 % of invasive adenocarcinomas. There were no differences among the three groups. The preinvasive lesions often presented as a smooth margin (70.00 %), while MIAs and invasive adenocarcinomas presented as a lobulated and spiculated margin (82.35 %, 90 %, respectively) (Figs. 3 and 4). Tumour-lung interface in three groups was shown to be as follows: well-defined (38.10 %) and ill-defined (61.90 %) in preinvasive lesions, well-defined (77.14 %) and ill-defined (22.86 %) in MIAs, and well-defined (86.84 %) and ill-defined (13.16 %) in invasive adenocarcinomas (Fig. 5). The air bronchogram was demonstrated in 9.52 % of preinvasive lesions, 20.00 % of MIAs, and 36.84 % of invasive adenocarcinomas (Fig. 6). Lesion shape, bubble sign and plural tag were not significantly different among the three groups ($P=0.17, P=$

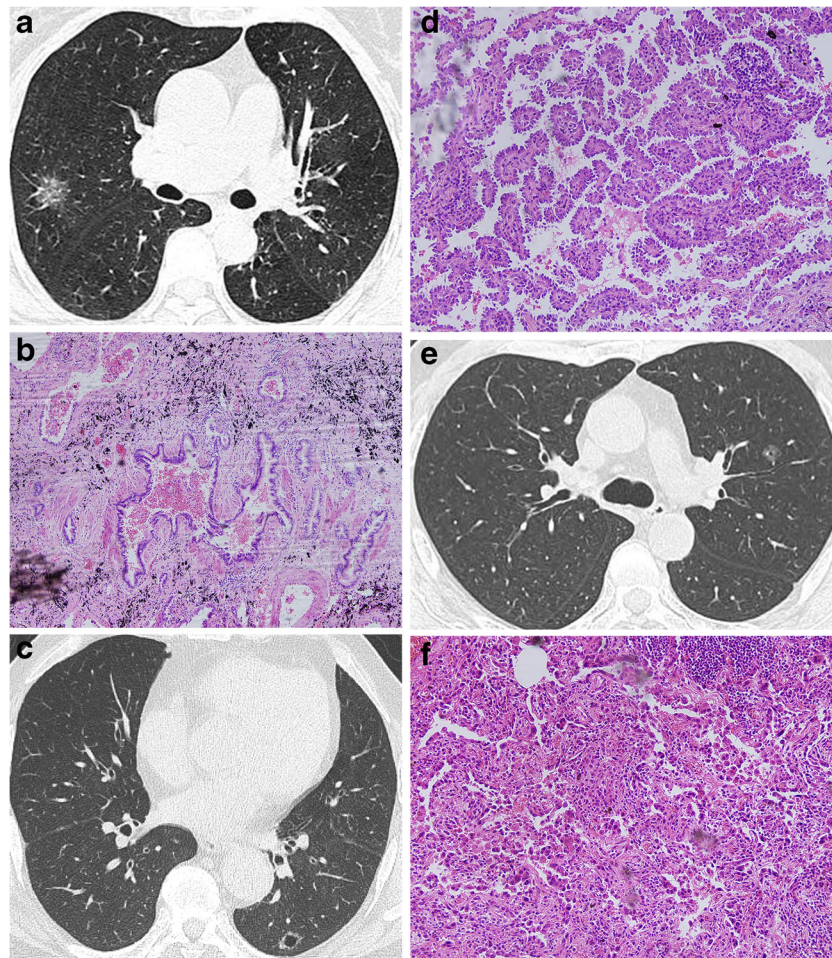


Fig. 7 Other subtypes of invasive adenocarcinoma, CT (transverse lung-window, thin-section 1.5 mm), and histopathologic photomicrograph (haematoxylin-eosin stain; magnification, B: $\times 40$; D,F: $\times 100$) (A) 1.5 mm thin-section CT scan of a 60-year-old woman showed a nodule with spiculation located in the right upper lobe. (B) Histopathology proved to be acinar predominant type, Haematoxylin-eosin stain (magnification, $\times 40$) showed a central luminal space surrounded by tumour cells. (C) Thin-section CT of a 69-year-old man showed a

nodule with spiculation and central large lucency located in the left lower lobe. (D) Histopathology proved to be a papillary predominant type, Haematoxylin-eosin stain (magnification, $\times 100$) showed malignant cuboidal to columnar tumour cells growing on the surface of fibrovascular cores. (E) A 6 mm nodule with bubble sign located in the left upper lobe in a 59-year-old man. (F) Histopathology proved to be poorly differentiated solid predominant type with cell degeneration

0.13, $P=0.66$, respectively, $P>0.05$) (Table 2). Some other subtypes of invasive adenocarcinoma are shown in Fig. 7.

Discussion

In our study, there were 38 (40 %) invasive adenocarcinomas presented as pGGO. Honda T et al. [5] reported that based on the new classification, invasive adenocarcinoma always presented as a solid component, but Lim HJ [6] and Lee SM [7] et al., both reported invasive adenocarcinoma as pGGO nodules, and 40 % of invasive adenocarcinoma appearing as pGGO in our study correlated very well with the results of Lim's report. Therefore, the CT characteristics for distinguishing preinvasive lesions from invasive adenocarcinoma appearing as pGGO nodules was of the most important results of the present study. This finding may potentially help the surgeon make a better selection of management of pGGO.

Kim HK and Lee HJ, et al. [8, 9] had shown that 8 mm was the optimal cut-off value for distinguishing benign from malignant pGGOs. Nakata et al. [10] reported that pGGOs of 10 mm or more in diameter were informative signs of malignancy. As for the new adenocarcinoma classification, Lee SM [7] showed that the optimal cut-off value for discriminating preinvasive lesions from IPAs (MIA and invasive adenocarcinoma) appearing as pGGOs was 10 mm and the specificity of the cut-off value was 100 %. We found that the optimal cut-off value for discriminating preinvasive lesions from invasive lesions (MIA and invasive adenocarcinoma) with pGGOs was 10.5 mm, and the positivity was 88.73 %, negativity was 56.52 %, and the specificity was 61.90 %. There were other authors [11, 12] who had reported cases of AAH larger than 10 mm in diameter. Lee SM [7] had mentioned the reason for the cut-off value being higher than in previous studies was that previous studies included BACs as malignant GGNs, whereas BAC, now referred to as AIS, was classified as a preinvasive lesion. In our study, there were several preinvasive lesions larger than 10 mm, and also invasive lesions less than 10 mm. This was why the specificity was lower (61.90 %) than that reported in Lee SM's report.

Our study showed that there were no significant differences in CT attenuation of pGGOs among the three groups. Previous studies had shown that CT attenuation had been suggested as an approach to differentiating different pathological types of lesions, and the higher the CT value, the more malignant the lesion was [13, 14]. Ikeda K et al. [13] reported AAH showed a one-peak pattern and AIS or MIA showed a two-peak pattern of attenuation. The difference between our study and previous studies can be explained by the fact that previous studies included pure GGO and part-solid GGO nodules, while pure GGO was the only subject in our study. There were significant differences in lesion uniformity between preinvasive lesions and MIAs or invasive adenocarcinomas

in our study ($P=0.01, P<0.05$), and the lesion uniformity was correlated with lesion size ($r=0.45$). Pathologically, with the tumour growing, dilated bronchiole and enlarged alveolar space were presented more [15], consequently, CT images appeared more heterogeneous. Regarding the morphologic CT features of pGGOs, there were no significant differences of shape among preinvasive lesions, MIAs, and invasive adenocarcinomas in our study, but some studies showed that a pGGO nodule with an oval appearance suggested a malignant nature and a polygonal shape indicated a benign nature [16–18], Kim HY [19] reported that no significant morphologic differences were observed in GGO nodules, so the shape of GGO was not a reliable CT sign for determining GGO natures. Our results demonstrated that the margin, tumour-lung interface, and air bronchogram were useful CT signs for indicating the histological invasiveness of pGGO nodules. A smooth margin was more common in preinvasive lesions, while MIAs and invasive adenocarcinomas appeared more likely as lobulated and spiculated nodules and with more air bronchogram signs, and, thus, our results correlated with previous studies [15, 20–22]. We also found that the more invasive extent of a lesion in pathology, the clearer was the border on CT, which may be explained histopathologically by the thickness of alveolar walls within the lesion. With the development of a lesion, the alveolar walls (including tumour cells and fibrous stroma) got thicker and thicker. Our study was limited by selection bias. We only included the pGGO nodules that underwent surgical resection, and those pGGO nodules may be considered to have the malignant tendency. This may explain why, when compared with previous reports [6, 7], our study contained a relatively greater percentage of pGGO invasive adenocarcinomas (40 %) and had four AAHs larger than 10 mm. Another limitation was the definition of lesion uniformity, which was not a widely accepted standard. The reliability of this definition needs further confirmation in the future. In conclusion, 40 % of resected pGGO lesions were invasive adenocarcinoma in our study. A value of 10.5 mm was the cut-off value for discriminating preinvasive lesions from invasive lesions. The lesion uniformity, tumour-lung interface, and the air bronchogram could indicate the invasive extent of early stage lung adenocarcinoma with pGGO.

Acknowledgments We would like to express special thanks to the doctors at the radiology department of PLA general hospital. The scientific guarantor of this publication is Zhao Shaohong. The authors of this manuscript declare no relationships with any companies, whose products or services may be related to the subject matter of the article. The authors state that this work has not received any funding. No complex statistical methods were necessary for this paper. Institutional Review Board approval was not required because this is a retrospective study. Written informed consent was not required for this study because this is a retrospective study. Approval from the institutional animal care committee was not required because this study is not on animals. Some study subjects or cohorts have not been previously reported. Methodology: retrospective, diagnostic or prognostic study, performed at one institution.

References

1. Ravenel JG (2012) Evidence-based imaging in lung cancer: a systematic review. *J Thorac Imaging* 27:315–324
2. Travis WD, Brambilla E, Noguchi M et al (2011) International association for the study of lung cancer/american thoracic society/european respiratory society international multidisciplinary classification of lung adenocarcinoma. *J Thorac Oncol* 6:244–285
3. Lee HJ, Lee CH, Jeong YJ et al (2012) IASLC/ATS/ERS International Multidisciplinary Classification of Lung Adenocarcinoma: novel concepts and radiologic implications. *J Thorac Imaging* 27:340–353
4. Godoy MC, Naidich DP (2012) Overview and strategic management of subsolid pulmonary nodules. *J Thorac Imaging* 27:240–248
5. Honda T, Kondo T, Murakami S et al (2013) Radiographic and pathological analysis of small lung adenocarcinoma using the new IASLC classification. *Clin Radiol* 68:e21–e26
6. Lim HJ, Ahn S, Lee KS et al (2013) Persistent Pure Ground-Glass Opacity Lung Nodules ≥ 10 mm in Diameter at CT: Histopathologic Comparisons and Prognostic Implications. *Chest* 144:1291–1299
7. Lee SM, Park CM, Goo JM, Lee HJ, Wi JY, Kang CH (2013) Invasive Pulmonary Adenocarcinomas versus Preinvasive Lesions Appearing as Ground-Glass Nodules: Differentiation by Using CT Features. *Radiology* 268:265–273
8. Kim HK, Choi YS, Kim K et al (2009) Management of ground-glass opacity lesions detected in patients with otherwise operable non-small cell lung cancer. *J Thorac Oncol* 4:1242–1246
9. Lee HJ, Goo JM, Lee CH et al (2009) Predictive CT findings of malignancy in ground-glass nodules on thin-section chest CT: the effects on radiologist performance. *Eur Radiol* 19:552–560
10. Nakata M, Saeki H, Takata I et al (2002) Focal ground-glass opacity detected by low-dose helical CT. *Chest* 121:1464–1467
11. Kawakami S, Sone S, Takashima S et al (2001) Atypical adenomatous hyperplasia of the lung: correlation between high-resolution CT findings and histopathologic features. *Eur Radiol* 11:811–814
12. Park CM, Goo JM, Lee HJ et al (2006) CT findings of atypical adenomatous hyperplasia in the lung. *Korean J Radiol* 7:80–86
13. Ikeda K, Awai K, Mori T, Kawanaka K, Yamashita Y, Nomori H (2007) Differential diagnosis of ground-glass opacity nodules: CT number analysis by three-dimensional computerized quantification. *Chest* 132:984–990
14. Godoy MC, Sabloff B, Naidich DP (2012) Subsolid pulmonary nodules: imaging evaluation and strategic management. *Curr Opin Pulm Med* 18:304–312
15. Fan L, Liu SY, Li QC, Yu H, Xiao XS (2011) Pulmonary malignant focal ground-glass opacity nodules and solid nodules of 3 cm or less: comparison of multi-detector CT features. *J Med Imaging Radiat Oncol* 55:279–285
16. Li F, Sone S, Abe H, Macmahon H, Doi K (2004) Malignant versus benign nodules at CT screening for lung cancer: comparison of thin-section CT findings. *Radiology* 233:793–798
17. Felix L, Serra-Tosio G, Lantuejoul S et al (2011) CT characteristics of resolving ground-glass opacities in a lung cancer screening programme. *Eur J Radiol* 77:410–416
18. Takashima S, Sone S, Li F et al (2003) Small solitary pulmonary nodules ($< \text{or} = 1$ cm) detected at population-based CT screening for lung cancer: Reliable high-resolution CT features of benign lesions. *AJR Am J Roentgenol* 180:955–964
19. Kim HY, Shim YM, Lee KS, Han J, Yi CA, Kim YK (2007) Persistent pulmonary nodular ground-glass opacity at thin-section CT: histopathologic comparisons. *Radiology* 245:267–275
20. Takashima S, Sone S, Li F, Maruyama Y, Hasegawa M, Kadoya M (2003) Indeterminate solitary pulmonary nodules revealed at population-based CT screening of the lung: using first follow-up diagnostic CT to differentiate benign and malignant lesions. *AJR Am J Roentgenol* 180:1255–1263
21. MacMahon H, Austin JH, Gamsu G et al (2005) Guidelines for management of small pulmonary nodules detected on CT scans: a statement from the Fleischner Society. *Radiology* 237:395–400
22. Kim TJ, Goo JM, Lee KW, Park CM, Lee HJ (2009) Clinical, pathological and thin-section CT features of persistent multiple ground-glass opacity nodules: comparison with solitary ground-glass opacity nodule. *Lung Cancer* 64:171–178